Tsunami signature in the ionosphere: A simulation of OTH radar observations

Pierdavide Coïsson, Giovanni Occhipinti, Philippe Lognonné, Jean-Philippe Molinié, Lucie Rolland

Tsunami signature in the ionosphere: A simulation of OTH radar observations

Pierdavide Coïsson,[1] Giovanni Occhipinti,[1] Philippe Lognonné,[1] Jean-Philippe Molinié,[2] and Lucie M. Rolland[1]

Received 27 December 2010; revised 15 July 2011; accepted 24 July 2011; published 22 October 2011.

[1] In the last ten years ionospheric anomalies following major earthquakes and tsunamis have been detected. Global Positioning System (GPS) and altimeters have been proven effective for this purpose, through Total Electron Content (TEC) measurement. Most of these ionospheric anomalies are deterministic and reproducible by numerical modeling via the coupling mechanism through ocean, neutral atmosphere and ionosphere. Numerical modeling supplies also useful support in the estimation of expected ionospheric effects and in the exploration and identification of new techniques to detect ionospheric tsunami signatures. We explore here a new ground-based technique, nominally the use of over-the-horizon (OTH) radars, for tsunami detection through ionospheric monitoring. OTH radars operate in High Frequency (HF) band and sounding the bottomside ionosphere they could anticipate the detection of tsunami-driven Internal Gravity Waves (IGW). To validate this hypothesis, we use HF numerical ray-tracing to simulate synthetic OTH radar measurements through a 3D tsunami-driven IGW ionospheric model. Our simulations clearly identify the tsunami signature in the OTH radar measurements one hour and a half before the tsunami arrival on the coast. The large coverage of OTH radar and its sensitivity to plasma anomalies open new perspectives in the oceanic monitoring and future tsunami warning systems.

Citation: Coïsson, P., G. Occhipinti, P. Lognonné, J.-P. Molinié, and L. M. Rolland (2011), Tsunami signature in the ionosphere: A simulation of OTH radar observations, *Radio Sci.*, *46*, RS0D20, doi:10.1029/2010RS004603.

1. Introduction

[2] After the first ionospheric observation performed by *Artru et al.* [2005] following the tsunamigenic earthquake in Peru (23 June 2001, M = 8.2), wide observational and theoretical evidence has confirmed that tsunamis are detectable by ionospheric monitoring. In essence, the oceanic surface displacement produced by tsunamis triggers atmospheric internal gravity waves (IGWs) that, propagating upward, are strongly amplified by the combined effect of decrease of density ρ and the conservation of kinetic energy $\rho v^2 = constant$; consequently, the small perturbation at the oceanic surface becomes huge when the IGWs reach ionospheric altitudes. The following interaction of IGWs with the ionosphere produces detectable perturbation on the plasma density and plasma velocity [*Hines*, 1972; *Peltier and Hines*, 1976; *Occhipinti et al.*, 2006, 2008a]. Ionospheric remote sensing, measuring the plasma velocity by Doppler sounders as well as measuring the total electron content (TEC) by altimeters or GPS, is able to detect tsunamis.

[3] The giant 2004 Sumatra earthquake and the following tsunami produced ionospheric anomalies observed from ground-based GPS measurements [*DasGupta et al.*, 2006; *Liu et al.*, 2006a; *Lognonné et al.*, 2006; *Astafyeva and Afraimovich*, 2006; *Otsuka et al.*, 2006; *Heki et al.*, 2006; *Occhipinti et al.*, 2008b; *Choosakul et al.*, 2009], HF Doppler sounders [*Liu et al.*, 2006b; *Occhipinti*, 2006] and space-based satellite altimeters [*Occhipinti et al.*, 2006; *Hao et al.*, 2006]. More recently, tsunamis triggered by the earthquakes in Kurils islands (15 November 2006), Samoa (29 September 2009) and Chile (27 February 2010) have produced ionospheric TEC anomalies detected offshore Hawaii using Hawaiian dense GPS networks [*Rolland et al.*, 2010]. Those results show that the tsunami signature in the ionosphere can be routinely detected.

[4] Additionally, the ionospheric anomalies are deterministic and reproducible by numerical modeling via the coupling mechanism through ocean, neutral atmosphere and ionosphere [*Occhipinti et al.*, 2006, 2008a; *Hickey et al.*, 2009; *Mai and Kiang*, 2009]. Consequently, the numerical modeling is useful in the estimation of expected anomalies, as well as to explore and identify new techniques to detect ionospheric tsunami signatures.

[1]Géophysique Spatiale et Planétaire, Institut de Physique du Globe de Paris–Sorbonne Paris Cité, Université Paris Diderot, UMR 7154 CNRS, France.
[2]Office National d'Etudes et de Recherches Aérospatiales, Palaiseau, France.

0048-6604/11/2010RS004603

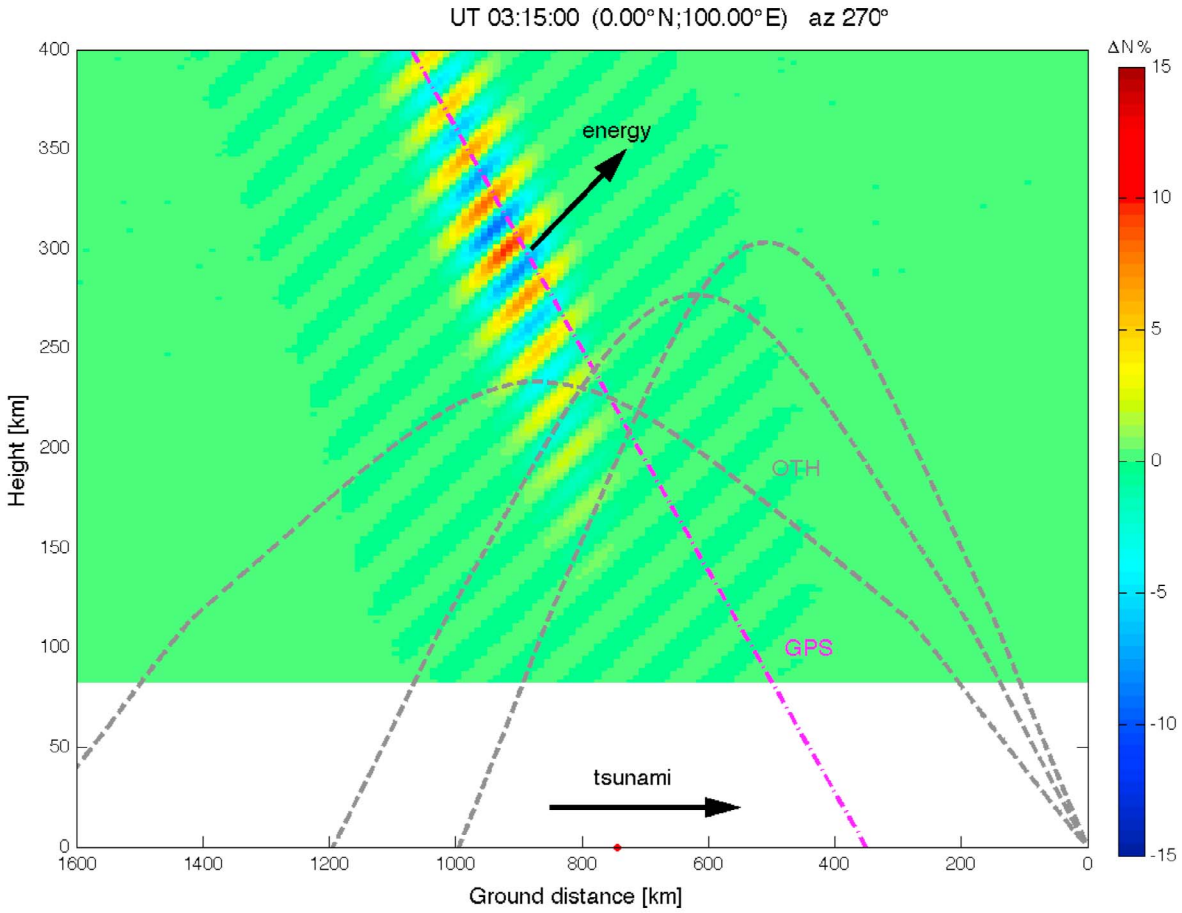

Figure 1. Vertical cross section of the modeled tsunami-driven electron density perturbation and raypaths computed using a 10 MHz OTH radar signal at 19°, 30° and 35° elevation (dashed gray lines). Dash-dotted purple line indicates a possible geometry of a GPS station for a satellite at 25° elevation. Arrows indicate the tsunami and IGW energy directions of propagation. Note that the vertical scale has been exaggerated.

[5] We also highlight that, despite altimeters clearly proving the link between tsunami propagation and the associated TEC perturbation [*Occhipinti et al.*, 2006], the observations are scarce and cannot be used for routine detection. Close to altimeters, dense GPS networks multiply the detection of tsunami related TEC perturbations [*Rolland et al.*, 2010]. Unfortunately, due to the integrated nature of TEC, the GPS measurements are strongly affected by the satellites-receivers geometry [*Rolland et al.*, 2010], as well as by the effect of geomagnetic field [*Occhipinti et al.*, 2008a]. After the 28 March 2005 Sumatra event it has been possible to detect the ionospheric signature of Rayleigh waves by OTH radar [*Occhipinti et al.*, 2010] in France, opening new opportunities of detection in ionospheric seismology. Therefore in this work, we explore the tsunami detection capability of over-the-horizon (OTH) radars by ionospheric monitoring.

2. Over-the-Horizon Radars

[6] Electromagnetic (EM) waves emitted in high frequency (HF) band (3–30 MHz) have the intrinsic property to be refracted by the ionosphere [e.g., *Davies*, 1989].

[7] The layered structure of the ionosphere produces a change of refractive index primarily as a function of altitude. OTH radars take advantage of this ionospheric refraction that bends HF rays progressively toward the ground to reach locations below the optical horizon.

[8] OTH radars are primarily designed for detection of hard targets (aircrafts and ships) for military purposes of air- and oceanic-areas monitoring in a range up to about 3000 km distance from the radar location. Additionally, existing OTH radars cover mostly sea-ocean areas, like the U.S. Navy Relocatable Over-the-Horizon Radars (ROTHR) [*Headrick and Thomason*, 1998], the Australian Jindalee Operational Radar Network (JORN) [*Anderson*, 2010], the French Nostradamus radar [*Bazin et al.*, 2006] or the Chinese radars [*Li*, 1998].

[9] Consequently, OTH radars are able to sound the ionosphere over oceanic areas at distances up to about 2000 km from the radar and could anticipate the detection of tsunami-driven IGW sounding the bottomside ionosphere. In essence, the propagation time variation of the emitted/detected EM waves is sensitive to the local electron density variations due to IGW propagation. It is therefore promising to analyze the OTH radar sensitivity to tsunami-driven IGW.

3. Modeling of Tsunami Detection by OTH

[10] Due to the small number of operational OTH radars and the need of a dedicated measurement campaign for detection of tsunami-driven IGW, there are currently no

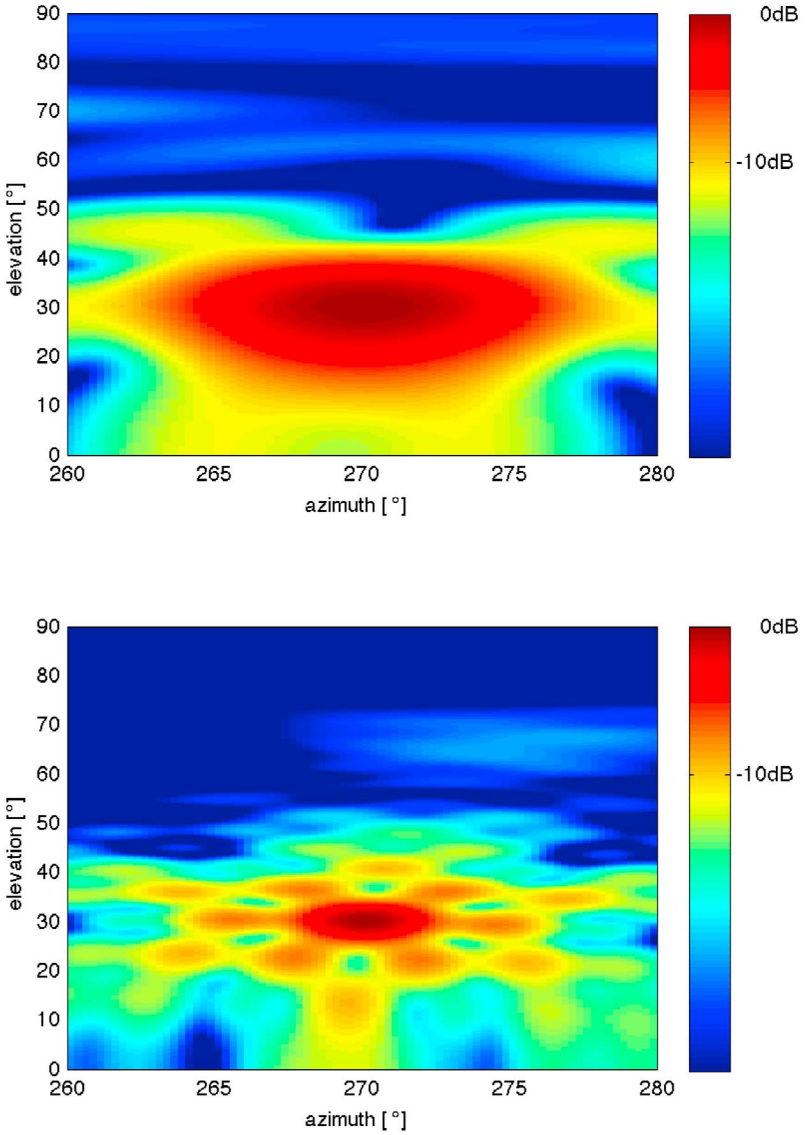

Figure 2. (top) OTH radar emission and (bottom) receiving patterns.

available OTH experimental observations of these ionospheric effects. Therefore a simulation approach is useful to explore the detection capability of OTH radar for this kind of waves. For this purpose, we simulate the detection by a monostatic OTH radar with similar characteristics of Nostradamus [*Bazin et al.*, 2006]. We use 3D HF ray-tracing technique [*Occhipinti*, 2006] to reproduce radar echoes. HF rays are computed propagating through a dynamic ionospheric model composed by both the background daily dynamics as well as the tsunami-driven IGW perturbation. Traveling Ionospheric Disturbances (TID) activity from other sources has not been included in this modeling to focus on the geometrical effects of the detection.

3.1. Ionospheric Perturbation

[11] The physical modeling results of *Occhipinti et al.* [2008a] show the characteristics of tsunami-driven IGW in term of horizontal and vertical propagation, geomagnetic field influence, electron density and TEC perturbation. Additionally, *Hickey et al.* [2009] include the attenuation characteristics with altitude. We use here a simplified ionospheric perturbation model, based on these results, to assess the response of an OTH radar to tsunami-driven IGWs. The attenuation effects of magnetic field and other geophysical perturbations are not included.

[12] The ambient electron density has been perturbed by a transverse wave with an amplitude that increases with altitude and fades out in the upper part of the ionosphere, coherently with previous work [e.g., *Occhipinti et al.*, 2008a]. We suppose that the horizontal phase velocity is constant with altitude and equal to the tsunami speed c:

$$c = \sqrt{gH} \tag{1}$$

where $g = 9.81\ m/s^2$ is the Earth gravity and H is the ocean depth.

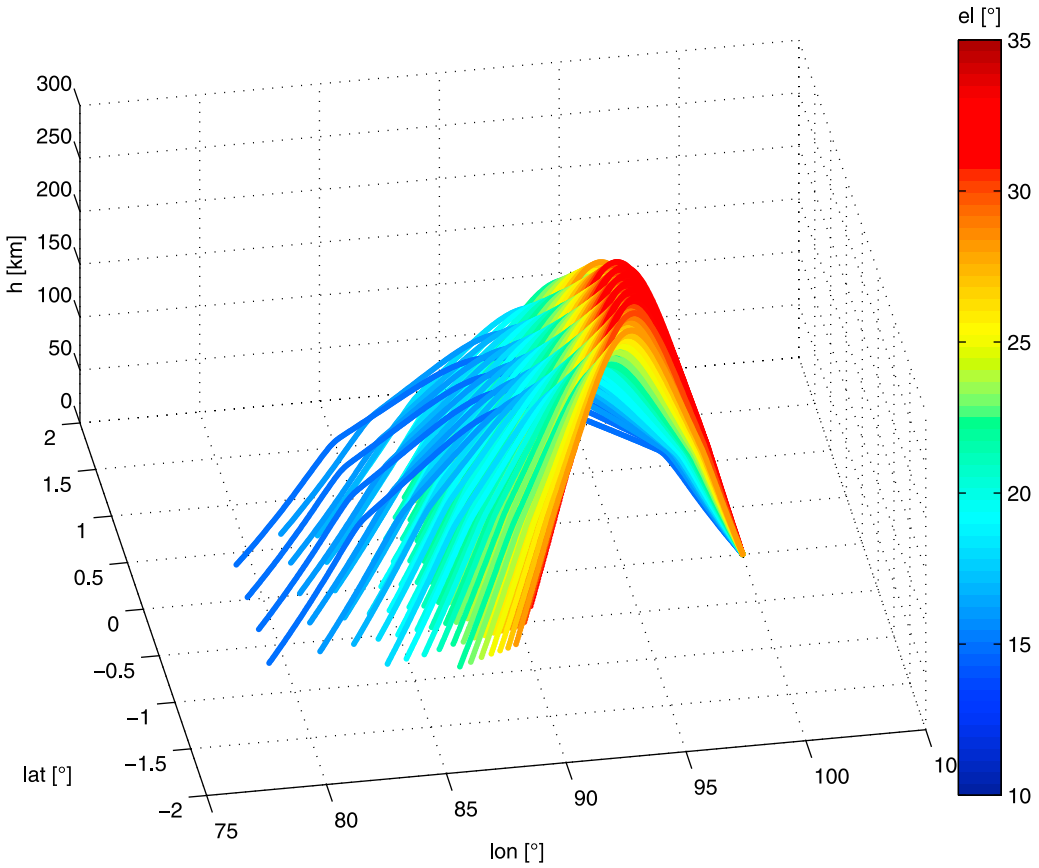

Figure 3. Example of raypaths in the discretized OTH emission pattern at 270° azimuth and 30° elevation. The color of each ray corresponds to its elevation angle at radar location.

[13] The wave is expressed in term of electron density perturbation $\Delta N/N$ and described as a sinusoidal function modulated by a Gaussian function:

$$\frac{\Delta N}{N} = A(z)\cos(\omega t - k_x x - k_z z)\exp - \frac{(\omega(t - dt(z)) - k_x x)^2}{2\sigma^2} \quad (2)$$

$$A(z) = \begin{cases} 0.1\sqrt{\dfrac{\rho(z_m)}{\rho(z)}} & \text{if } z \le z_m \\ 0.1\sqrt{\dfrac{\rho(z_m)}{\rho(z)}}\exp\left(-\dfrac{z - z_m}{\zeta}\right) & \text{if } z > z_m \end{cases} \quad (3)$$

where ω is the angular frequency, k_x is the horizontal wave number, k_z vertical wave number, σ is the width of the Gaussian window and $dt(z)$ represents the delay of the IGW wave as function of height, following the modeling results of *Occhipinti et al.* [2011]. The amplitude A(z) of the electron density perturbation is modulated by the neutral atmosphere density $\rho(z)$ and reaches its maximum at z_m = 300 km height, where a 10% perturbation of the background electron density is assumed. Above that height the wave amplitude decreases exponentially with scale height ζ = 50 km to reproduce the effect of the atmosphere viscosity, thermo-conduction and ion drag that intervene in keeping the maximum perturbation within the F2 region [*Hickey et al.*, 2009]. Our model of ionospheric perturbation has been used to simulate a tsunami-driven IGW event above the Indian Ocean applying the atmospheric and ionospheric climatological conditions of December 2004 based on NRLMSISE-00 neutral atmosphere density ρ (z) model [*Picone et al.*, 2002] and NeQuick electron density model [*Nava et al.*, 2008]. The synthetic radar has been located at (0°N 100°E) and the origin of the wave at (0°N 80°E) at 01:00 UT. During the simulation interval of 4 hours it was local morning, the ionosphere was developing under the influence of solar radiation: solar flux F10.7 input for the models was 91.7 solar flux units (1 sfu = 10^{-22} Wm^{-2} Hz^{-1}). The wave has been propagated radially from the source at the speed of 182 m/s (corresponding to an ocean depth of 3400 m).

[14] We simulated an ionospheric IGW with a 10 minutes period, corresponding to a tsunami period suggested by previous works [*Occhipinti et al.*, 2008a; *Rolland et al.*, 2010]. The vertical speed of this IGW is in the order of 55 m/s, corresponding to a mean value of tsunami-driven IGW vertical propagation.

[15] An example of vertical cross section of electron density perturbation is given in Figure 1, along with computed radar raypaths crossing the region affected by the IGW (the complete simulation sequence is available in Animation S1 of the auxiliary material).[1]

[1] Auxiliary materials are available in the HTML. doi:10.1029/2010RS004603.

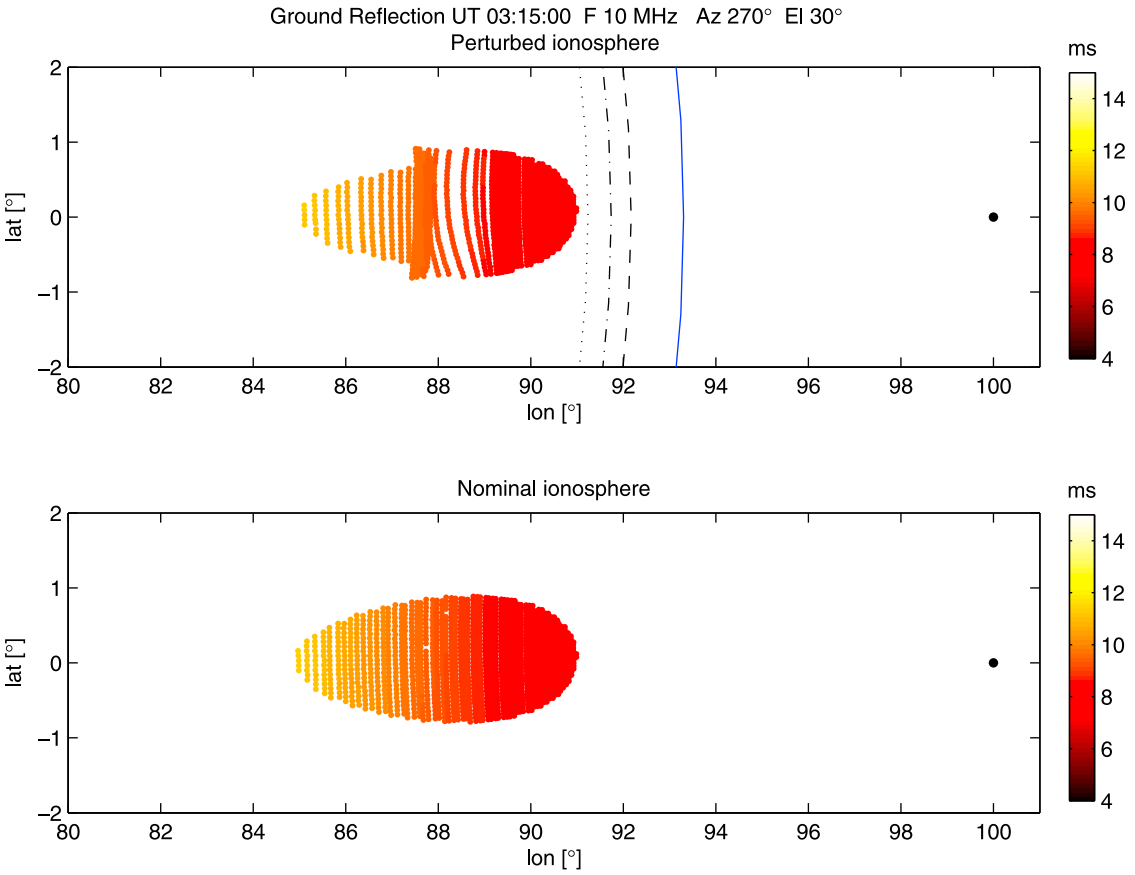

Figure 4. Location of rays' endpoints at ground level for 270° azimuth and 30° elevation at 03:15 UT. Color scale is the rays' travel time. (top) IGW perturbed ionosphere, the black dot indicates the location of the simulated radar, the blue line is the position of the tsunami and the black curves the position of the wavefronts at 350, 300, and 250 km height from left to right. (bottom) Arrival points through undisturbed ionosphere.

3.2. Observational Geometry and Ionosphere Response

[16] In Figure 1 we compare OTH radar raypaths with GPS line of sight. GPS-TEC observations are constrained by the satellites positions and, as a consequence of the integrated nature of TEC, their sensitivity to perturbations is maximum near the ionosphere F2 peak at around 350 km height, an altitude where the coupling between the IGW and the ionosphere is strongly affected by the geomagnetic field. Modeling by *Occhipinti et al.* [2008a] clearly shows that this geomagnetic field dependence induces an amplification of the electron density perturbation in the equatorial region. This fact suggests that tsunami detection by GPS-TEC is less favorable at high latitudes. It was also shown that at E region altitude the electron density perturbation is not affected by the magnetic field.

[17] OTH radars strictly sound the bottomside ionosphere from the E region at around 100 km to the lower F2 region where reflections take place usually below 300 km, depending on the elevation angle. Consequently, ionospheric detection of tsunami-driven IGW by OTH radar is less affected by the geomagnetic latitude location than GPS-TEC.

[18] Another advantage of OTH radar comes from the possibility to aim the radar soundings at a chosen direction and therefore also in the arrival direction of the incoming gravity wave, based on the epicenter location of tsunamigenic earthquakes. As shown in Figure 1, tsunami-driven gravity waves have phase planes oriented in the orthogonal direction of the group velocity [*Nappo*, 2002]. Therefore an observational geometry that is parallel to these planes is more sensitive to the ionospheric perturbation [*Rolland*, 2010]. For coastal warning we note that OTH radar have their downward legs of signal propagation crossing the ionospheric perturbations in the direction of the phase planes, while GPS cannot achieve such geometry from the same location. The directions of maximum sensitivity for IGW detection by GPS-TEC are located in the downstream part of tsunami propagation.

3.3. Simulation of Radar Emission and Reception Patterns

[19] OTH radars emission patterns extend over large areas (Figure 2), therefore a key point of this work is to understand if the IGW signature in the OTH radar echoes could be recognized notwithstanding the broad emission beam.

[20] To achieve this objective, we made a 3D full OTH radar simulation discretizing the emission pattern of the emitting antennas. Then, we used the 3D HF radio ray-tracing technique [*Occhipinti*, 2006] to compute the travel

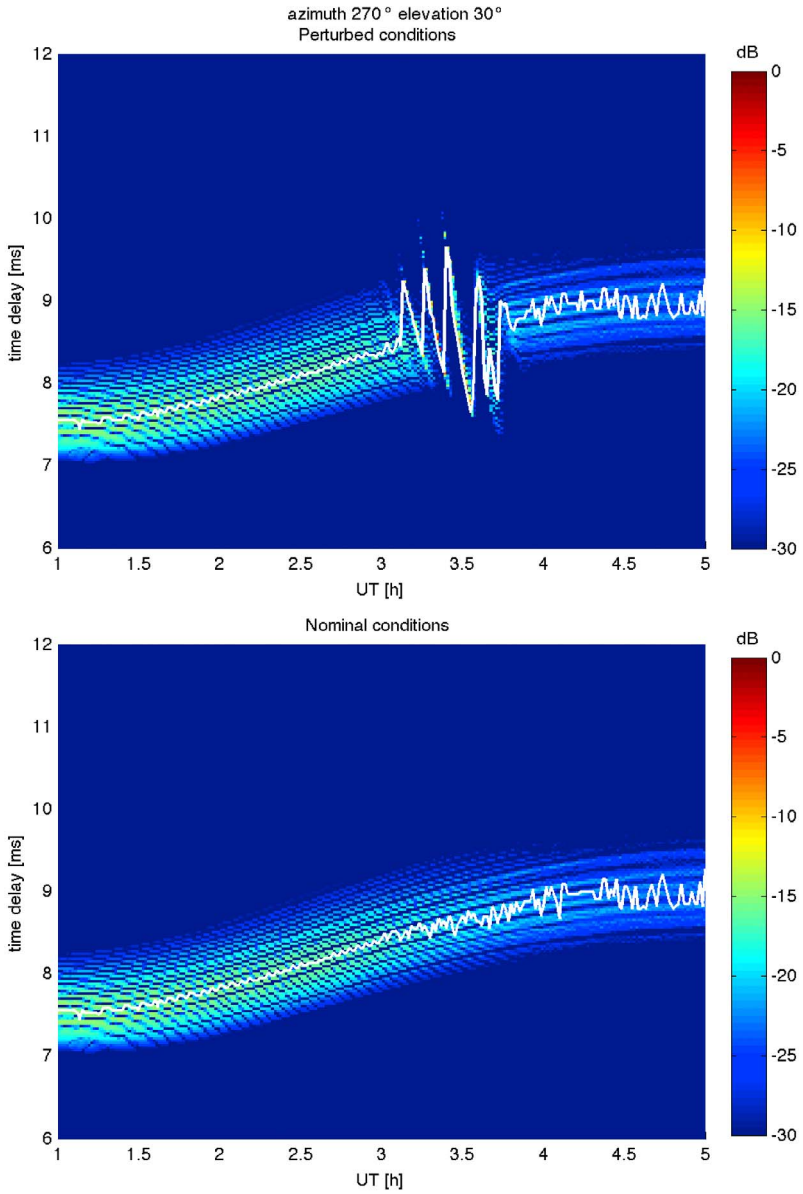

Figure 5. Synthetic OTH radar record from 01:00 to 05:00 UT at 270° azimuth 30° elevation. (top) Ionosphere with IGW perturbation and (bottom) unperturbed ionosphere. The signal strength is normalized to the maximum received during the whole observation period. White points indicate the maximum signal strength at each UT.

time along each ray direction on a 0.25° × 0.25° grid around the radar pointing direction up to −6 dB level.

[21] Figure 3 shows the computed raypaths in the emission pattern at 30° elevation angle, illustrating the variation of ionospheric reflection height. Rays with higher elevation angle are reflected at higher altitude sounding the ionosphere more deeply in the F2 region, while rays with lower elevation angle are reflected at lower altitudes and reach more distant ground locations.

[22] The calculation of radar echoes travel time is done assuming a monostatic radar configuration (co-located emission and reception) and that the same raypath is followed by the emitted radar signal and by the backscattered signal after ground reflection.

[23] In our simulation the sea surface reflectivity and the atmospheric absorption have not been taken into account.

[24] After setting a time resolution for the radar listening time, we computed the radar recorded power considering the energy carried by each ray according to its travel time. We took into account the radar emission power, the free-space-loss and the received power according to the radar patterns. The OTH radar Nostradamus uses a larger number of antennas in reception than in emission, therefore the receiving pattern is narrower than the emission pattern and allows higher resolution detection in several areas covered by a single emission pattern.

[25] To obtain a parameterization of the response of OTH radar we computed 4 hours of simulations with a time resolution

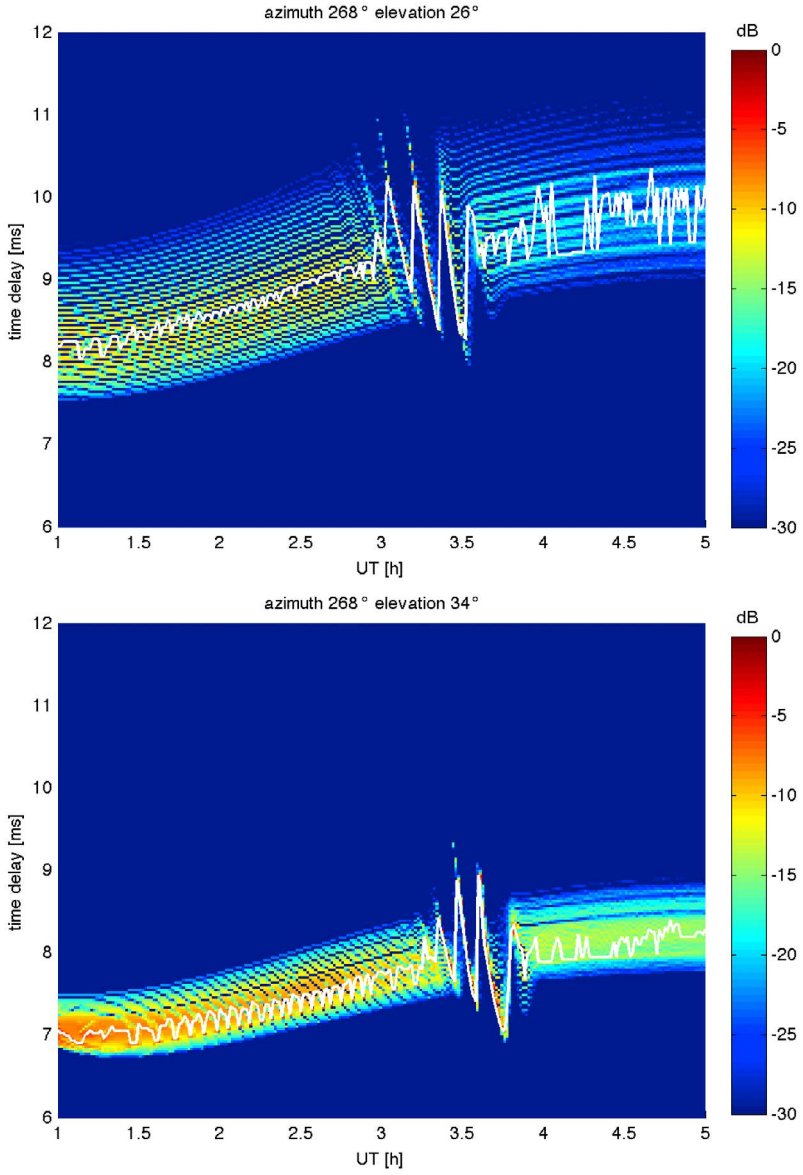

Figure 6. Synthetic OTH radar record from 01:00 to 05:00 UT at 268° azimuth. (top) Elevation 28° and (bottom) elevation 34°. The signal strength is normalized to the maximum received during the whole observation period. White points indicate the maximum signal strength at each UT.

of 1 minute. This resolution is enough to discriminate tsunami-driven IGWs, however we note that radar echoes are available every 20 ms. Consequently the real time resolution is 3000 times higher than the resolution used here.

[26] Both unperturbed and IGW perturbed ionosphere from 01:00 UT to 05:00 UT have been analyzed for an emission pattern centered at 270° azimuth and 30° elevation, aiming at the direction of the source of the IGW. The operating frequency considered was 10 MHz, suitable for far distance observation at the local time of the simulation.

[27] Observing the rays endpoints it is possible to appreciate the deflection due to crossing region where the plasma have been moved by the IGW (Figure 4 and Animation S2). This effect is stronger in the down-leg of the rays, when the ray is nearly parallel to the wavefronts. The IGW wavefronts at ionospheric heights are found between the radar and the ray endpoints. The redistribution of the endpoints occurs along directions that are parallel to them, as evident from the comparison with rays computed through unperturbed ionosphere.

[28] Figure 5 shows the radar synthetic observation for azimuth 270°, in the direction of arrival of the IGW. The variation of the ionosphere in the morning hours is seen as a slow increase of the radar echo time in the first three hours of the simulation. Starting shortly after 03:00 UT a sawtooth perturbation is observed moving from the upper part of the figure and lasting nearly 40 minutes. This effect can be seen also at other receiving directions (Figure 6). For 26° elevation angle the radar is observing a more distant and larger area and a strong perturbation is observed starting 10 minutes earlier.

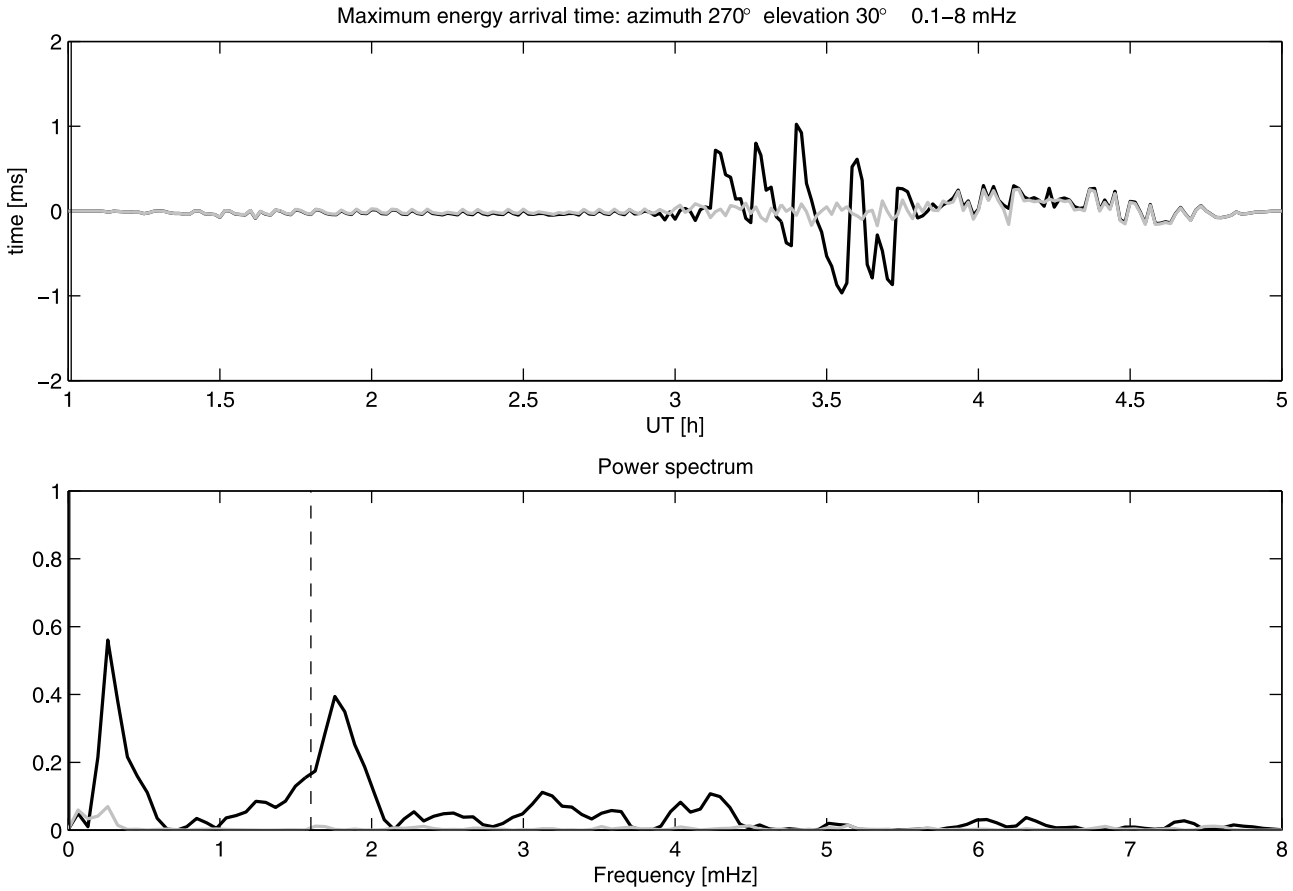

Figure 7. (top) Filtered time series and (bottom) power spectrum of the arrival time of radar echo maximum at 270° azimuth 30° elevation, showing a peak near 1.6 mHz corresponding to the IGW frequency. Black: perturbed ionosphere, gray: nominal conditions. During the time when the perturbation is not crossing the area sounded by the radar the two curves are superimposed.

34° elevation covers a closer and narrower region and the ionospheric reflection points is near to the maximum electron density perturbation. Here the perturbation becomes clear around 03:15 UT and its amplitude increases during the following half hour, before it disappears.

3.4. OTH Signal Analysis

[29] Tracking the arrival time of the maximum signal strength at the radar for each UT we obtained a time series that has been band-pass filtered between 0.1 and 8 mHz using a two-pass three-pole Butterworth filter to study its power spectrum. Despite the noise due to the emission pattern discretization, a clear signature is observed near 1.6 mHz in the perturbed simulation (Figure 7), corresponding to the frequency of the synthetic IGW. It is also seen that only the time interval between 03:00 and 03:45 UT is affected by the IGW. Repeating the same analysis for other OTH receiving patterns at higher and lower elevations, the signature of the IGW is detected in the same way, being observable later for higher elevations (see Figure 8). This signature can be observed within an azimuth range of about 40°. In this simulation the tsunami arrival time at the shoreline near the OTH location is about 04:30 UT, more than one hour and half after the first recorded ionospheric perturbation at 30° elevation. Lowering the elevation angle, it can be expected that in real conditions the detection could occur even earlier.

4. Conclusions

[30] The analysis of tsunami-driven ionospheric perturbation observed after major events provides valuable information for understanding the physical processes and explore new techniques for tsunami warning systems. We have shown here that early detection of tsunami-driven IGWs is possible using OTH radar backscattered echoes. The ray tracing simulation through a perturbed ionosphere by a traveling IGW induced by tsunami showed that it is possible to observe clearly the tsunami signature in the radar echoes. In the present study the effects of winds or the presence of other TIDs or ionospheric irregularities that could affect the detection efficiency have not been modeled to focus on the geometrical aspects of OTH radar detection. The detection efficiency of the ionospheric perturbation depends on the angle between the IGW wavefront and the radar-pointing azimuth and elevation as well as on the ionospheric environmental conditions. The observation in the direction of approaching tsunami shows a clear signature in the OTH radar echoes appearing one hour and half before the tsunami arrival.

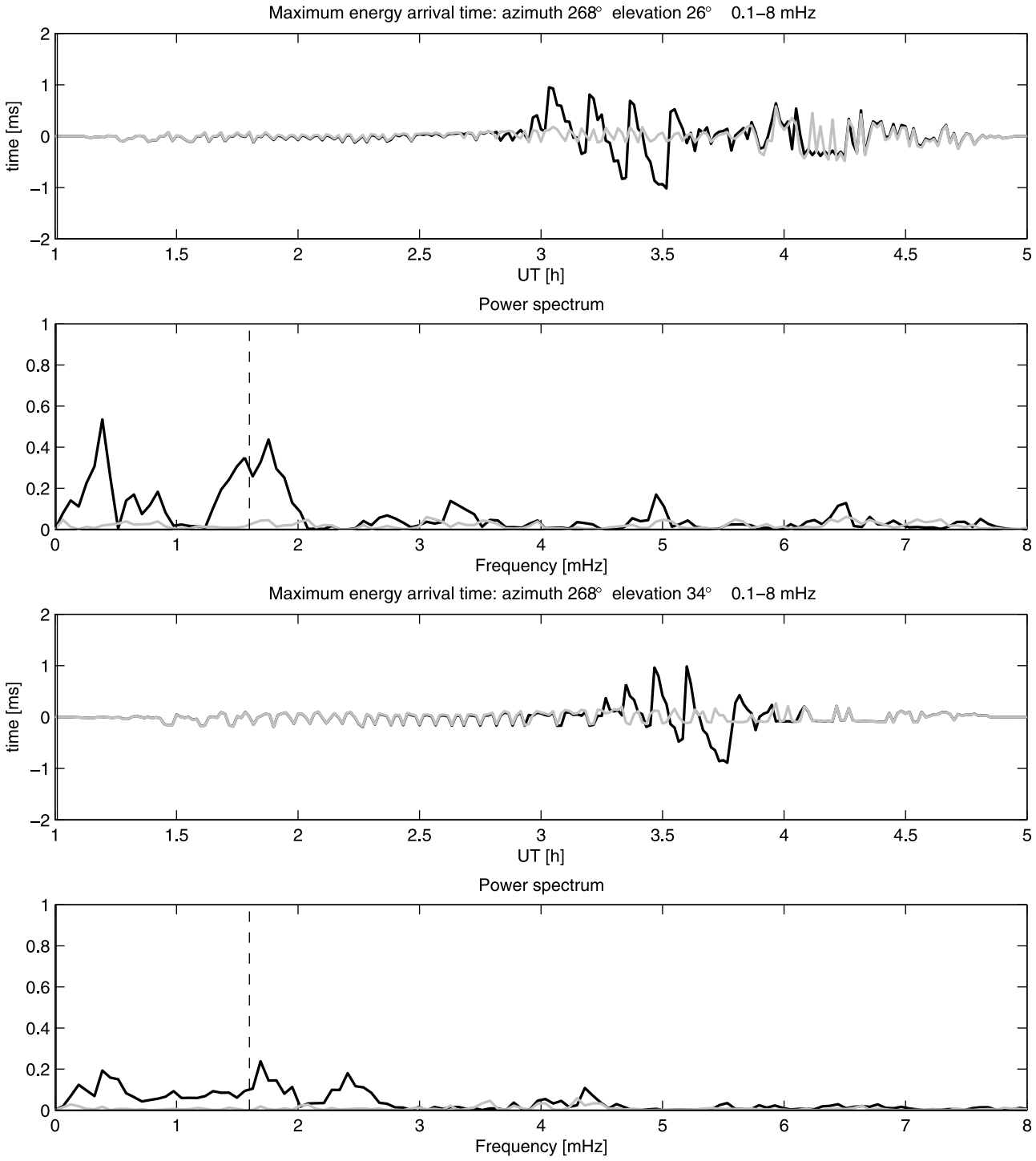

Figure 8. (top to bottom) Filtered time series, power spectrum of the arrival time of radar echo maximum at 268° azimuth, 28° elevation and filtered time series and power spectrum of the arrival time at 34° elevation, showing a peak near 1.6 mHz corresponding to the IGW frequency. Black: perturbed ionosphere, gray: nominal conditions. During the time when the perturbation is not crossing the area sounded by the radar the two curves are superimposed.

[31] These results open new perspectives in tsunami detection and strongly encourage experimental studies on over-the-horizon radars to include these powerful instruments in future tsunami warning systems.

[32] **Acknowledgments.** This project is supported by the United States (U.S.) Office of Naval Research (ONR) Global under contract IONONAMI-N07-25 with additional and early support from Centre National d'Etudes Spatiales (CNES), Agence Nationale de la Recherche (ANR) and Programme National de Télédétection Spatiale of Institut

National des Sciences de l'Univers (PNTS/INSU). We thank Office National d'Etudes et Recherches Aérospatiales (ONERA) staff for fruitful technical discussions and software on OTH radar. We thank the Aeronomy and Radiopropagation Laboratory of the Abdus Salam International Centre for Theoretical Physics (ICTP) for the use of NeQuick 2 model. We thank Tiger J. Y. Liu and two anonymous reviewers for constructive comments. This is IPGP contribution 3199.

References

Anderson, S. J. (2010), Remote sensing applications of HF skywave radar: The Australian experience, *Turk. J. Electr. Eng. Comput. Sci.*, *18*(3), 339–372.

Artru, J., V. Ducic, H. Kanamori, P. Lognonné, and M. Murakami (2005), Ionospheric detection of gravity waves induced by tsunamis, *Geophys. J. Int.*, *160*(3), 840–848.

Astafyeva, E. I., and E. L. Afraimovich (2006), Long-distance traveling ionospheric disturbances caused by the great Sumatra-Andaman earthquake on 26 December 2004, *Earth Planets Space*, *58*, 1025–1031.

Bazin, V., J.-P. Molinie, J. Munoz, P. Dorey, S. Saillant, G. Auffray, V. Rannou, and M. Lesturgie (2006), Nostradamus: An OTH radar, *IEEE Aerosp. Electron. Syst. Mag.*, *21*(10), 3–11, doi:10.1109/MAES.2006.275299.

Choosakul, N., A. Saito, T. Iyemori, and M. Hashizume (2009), Excitation of 4-min periodic ionospheric variations following the great Sumatra-Andaman earthquake in 2004, *J. Geophys. Res.*, *114*, A10313, doi:10.1029/2008JA013915.

DasGupta, A., A. Das, D. Hui, K. K. Bandyopadhyay, and M. R. Sivaraman (2006), Ionospheric perturbations observed by the GPS following the December 26th, 2004 Sumatra-Andaman earthquake, *Earth Planets Space*, *58*, 167–172.

Davies, K. (1989), *Ionospheric Radio*, Peter Peregrinus, London.

Hao, Y.-Q., Z. Xiao, and D.-H. Zhang (2006), Responses of the ionosphere to the great Sumatra earthquake and volcanic eruption of Pinatubo, *Chin. Phys. Lett.*, *23*(7), 1955–1957.

Headrick, J. M., and J. F. Thomason (1998), Applications of high-frequency radar, *Radio Sci.*, *33*(4), 1045–1054, doi:10.1029/98RS01013.

Heki, K., Y. Otsuka, N. Choosakul, N. Hemmakorn, T. Komolmis, and T. Maruyama (2006), Detection of ruptures of Andaman fault segments in the 2004 great Sumatra earthquake with coseismic ionospheric disturbances, *J. Geophys. Res.*, *111*, B09313, doi:10.1029/2005JB004202.

Hickey, M. P., G. Schubert, and R. L. Walterscheid (2009), Propagation of tsunami-driven gravity waves into the thermosphere and ionosphere, *J. Geophys. Res.*, *114*, A08304, doi:10.1029/2009JA014105.

Hines, C. O. (1972), Gravity waves in the atmosphere, *Nature*, *239*, 73–78.

Li, L.-W. (1998), High-frequency over-the-horizon radar and ionospheric backscatter studies in China, *Radio Sci.*, *33*(5), 1445–1458, doi:10.1029/98RS01606.

Liu, J.-Y., Y.-B. Tsai, K.-F. Ma, Y.-I. Chen, H.-F. Tsai, C.-H. Lin, M. Kamogawa, and C.-P. Lee (2006a), Ionospheric GPS total electron content (TEC) disturbances triggered by the 26 December 2004 Indian Ocean tsunami, *J. Geophys. Res.*, *111*, A05303, doi:10.1029/2005JA011200.

Liu, J. Y., Y. B. Tsai, S. W. Chen, C. P. Lee, Y. C. Chen, H. Y. Yen, W. Y. Chang, and C. Liu (2006b), Giant ionospheric disturbances excited by the M9.3 Sumatra earthquake of 26 December 2004, *Geophys. Res. Lett.*, *33*, L02103, doi:10.1029/2005GL023963.

Lognonné, P., J. Artru, R. Garcia, F. Crespon, V. Ducic, E. Jeansou, G. Occhipinti, J. Helbert, G. Moreaux, and P. Godet (2006), Ground-based GPS imaging of ionospheric post-seismic signal, *Planet. Space Sci.*, *54*(5), 528–540, doi:10.1016/j.pss.2005.10.021.

Mai, C.-L., and J.-F. Kiang (2009), Modeling of ionospheric perturbation by 2004 Sumatra tsunami, *Radio Sci.*, *44*, RS3011, doi:10.1029/2008RS004060.

Nappo, C. J. (2002), *An Introduction to Atmospheric Gravity Waves*, *Int. Geophys. Ser.*, vol. 85, Academic, San Diego, Calif.

Nava, B., P. Coïsson, and S. Radicella (2008), A new version of the NeQuick ionosphere electron density model, *J. Atmos. Sol. Terr. Phys.*, *70*(15), 1856–1862.

Occhipinti, G. (2006), Observations multi-paramètres et modélisation de la signature ionosphérique du grand séisme de Sumatra, Ph.D. thesis, Inst. de Phys. du Globe de Paris, Paris.

Occhipinti, G., P. Lognonné, E. A. Kherani, and H. Hébert (2006), Three-dimensional waveform modeling of ionospheric signature induced by the 2004 Sumatra tsunami, *Geophys. Res. Lett.*, *33*, L20104, doi:10.1029/2006GL026865.

Occhipinti, G., E. A. Kherani, and P. Lognonné (2008a), Geomagnetic dependence of ionospheric disturbances induced by tsunamigenic internal gravity waves, *Geophys. J. Int.*, *173*(3), 753–756, doi:10.1111/j.1365-246X.2008.03760.x.

Occhipinti, G., A. Komjathy, and P. Lognonné (2008b), Tsunami detection by GPS, *GPS World*, 1 Feb., 50–56. [Available at http://www.gpsworld.com/gps-world-issue/february-1-2008-696.]

Occhipinti, G., P. Dorey, T. Farges, and P. Lognonné (2010), Nostradamus: The radar that wanted to be a seismometer, *Geophys. Res. Lett.*, *37*, L18104, doi:10.1029/2010GL044009.

Occhipinti, G., P. Coïsson, J. J. Makela, S. Allgeyer, A. Kherani, H. Hébert, and P. Lognonné (2011), Three-dimensional numerical modeling of tsunami-related internal gravity waves in the Hawaiian atmosphere, *Earth Planets Space*, *63*, doi:10.5047/eps.2011.06.051, in press.

Otsuka, Y., et al. (2006), GPS detection of total electron content variations over Indonesia and Thailand following the 26 December 2004 earthquake, *Earth Planets Space*, *58*, 159–165.

Peltier, W. R., and C. O. Hines (1976), On the possible detection of tsunamis by a monitoring of the ionosphere, *J. Geophys. Res.*, *81*(12), 1995–2000, doi:10.1029/JC081i012p01995.

Picone, J. M., A. E. Hedin, D. P. Drob, and A. C. Aikin (2002), NRLMSISE-00 empirical model of the atmosphere: Statistical comparisons and scientific issues, *J. Geophys. Res.*, *107*(A12), 1468, doi:10.1029/2002JA009430.

Rolland, L. (2010), Sismologie ionosphérique: Détection et modélisation des ondes ionosphériques postsismiques, Ph.D. thesis, Inst. de Phys. du Globe de Paris, Paris.

Rolland, L. M., G. Occhipinti, P. Lognonné, and A. Loevenbruck (2010), Ionospheric gravity waves detected offshore Hawaii after tsunamis, *Geophys. Res. Lett.*, *37*, L17101, doi:10.1029/2010GL044479.

P. Coïsson, P. Lognonné, G. Occhipinti, and L. M. Rolland, Géophysique Spatiale et Planétaire, Institut de Physique du Globe de Paris-Sorbonne Paris Cité, Université Paris Diderot, UMR 7154 CNRS, 4 Avenue de Neptune, F-94100 Saint-Maur des Fossés, France. (coisson@ipgp.fr; ninto@ipgp.fr)

J. P. Molinié, Office National d'Etudes et de Recherches Aérospatiales, F-91761 Palaiseau, France.